Hindawi
Journal of Nanomaterials
Volume 2022, Article ID 9452318, 17 pages
https://doi.org/10.1155/2022/9452318

Research Article

Electrospun 1D and 2D Carbon and Polyvinylidene Fluoride (PVDF) Piezoelectric Nanocomposites

Hang Song,[1,2] Wenhui Song,[3] Jin-hua Song,[2] Virginia Martin Torrejon,[4] and Qinxiang Xia[1]

[1]*School of Mechanical and Automotive Engineering, South China University of Technology, Guangzhou 511442, China*
[2]*School of Innovation and Entrepreneurship, Southern University of Science and Technology, Shenzhen 518055, China*
[3]*Department of Surgical Biotechnology, University College London, London NW3 2PF, UK*
[4]*Media and Communication School, Shenzhen Polytechnic, Shenzhen 518055, China*

Correspondence should be addressed to Qinxiang Xia; meqxxia@scut.edu.cn

Received 18 December 2021; Revised 17 February 2022; Accepted 26 March 2022; Published 30 April 2022

Academic Editor: Bhanu P. Singh

Piezoelectric nanocomposite fibrous membranes consisting of polymer polyvinylidene fluoride (PVDF) as matrix and incorporating 1D carbon nanotubes (CNTs) and 2D graphene oxide (GO) were prepared using an electrospinning process. The influence of the filler type, loading, and dispersion status on the total PVDF crystallinity (X_c); the relative fraction of the β phase (piezoelectric phase) in crystalline PVDF (F_β); the volume fraction of β phase in the samples (v_β); and the piezoelectric coefficient d_{33} were investigated. The v_β is used to assess the formation of β phase for the first time, which considered the combined influence of fillers on X_c and F_β, and is more practical than other investigations using only F_β for the assessment. The inclusion of all types of carbon fillers had resulted in a considerable reduction in the X_c compared with the neat PVDF, and the X_c decreased with the CNT loading while increased with the GO loading. The addition of CNT and GO had also reduced the F_β compared with the neat PVDF, and F_β increased with CNT loading while decreased as GO loading increased. The v_β is significantly reduced by the addition of CNT and GO, while v_β decreases with CNT and GO loading increases. Since the calculation of v_β has considered the combined influence of fillers on X_c and F_β, both of which were reduced by incorporating CNT and GO, the reduction of v_β was expected. The v_β of the PVDF/CNT composites were higher than that of the PVDF/GO composites. Although it is generally anticipated that d_{33} increases with v_β, it is observed that in the presence of CNT, d_{33} is dominated by the increase in electric conductivity of the composites during and after the electrospinning process, giving rise to transport of charges, produced by β crystals within the fiber to the surface of the sample. In addition, the 1D CNTs may have promoted the orientation of β crystals in the d_{33} direction, therefore, enhancing the d_{33} of the composites despite the hindrance of the β-phase formation (i.e., the reduction of v_β). Adding CNTs can also improve piezoelectricity through interfacial polarization, which increases the dielectric constant of composite (mobile charges within CNTs facilitate composite polarization). CNT loadings higher than 0.01 wt.% are sufficient to outperform the neat PVDF, and d_{33} becomes 59.7% higher than the neat PVDF at 0.03 wt.% loading, but only GO loadings of 0.5 wt.% achieved comparable d_{33} to the neat PVDF; further increase in GO loading had resulted in a decline in d_{33}. The low conductivity of GO, the influence of flocculation, and the lower aspect ratio compared with CNT may result in lower electron transfer and less orientation of the β-phase polycrystalline. The d_{33} of the PVDF/CNT composites is higher than that of the PVDF/GO composites despite much higher loading of GO. This study aims to contribute to the development of PVDF nanocomposites in piezoelectric energy harvesting applications (e.g., self-powered biosensors and wireless sensor networks).

1. Introduction

Piezoelectricity of poled polyvinylidene fluoride (PVDF) thin films was observed with a higher piezoelectric coefficient (6–7 pC/N) than other organic or polymeric counterparts [1]. PVDF has four different crystalline phases depending on the packing structures of different chain conformations: α or δ (TGTG′), β (TTTT), and γ (TTTGTT TG′) (T-trans, G-gauche+, and G′-gauche–). Generally speaking, the α phase is more kinetically favorable, and therefore, normal crystallization from the melt and solution casting from nonpolar solvents typically result in α phase. The δ phase is a polar polymorph of the α phase [2]. The γ phase can be obtained by either solution-casting from strongly polar solvents or crystallization at high temperatures [3, 4]. The β phase in PVDF is more thermodynamically stable and possesses piezoelectricity because it shows spontaneous polarization and has a pure dipole moment. The β phase has the highest polarization per unit cell, which makes it the highly polarizable and causes the strongest piezoelectric properties and highest piezoelectric coefficient [5–7]. The nonpiezoelectric α phase and γ phase could be converted to β phase by poling under high electric fields or mechanical stretching [8].

Electrospinning has attracted great attention as a simple and versatile technique to manufacture various ultrafine fibers at 10s to 100 s nanometers in diameter that are difficult to achieve by other methods. It has been used to prepare ultrafine fibers from polymers, ceramics, composites, and metals in the form of a solution or melt [9]. Electrospinning produces ultrafine fibers by extensional forces generated under high electrostatic voltages (~10–20 kV), which essentially combines electrical poling and uniaxial stretching in one-step attributed to the promotion of β-phase formation. The mechanical uniaxial stretching contributes to the transition of the original spherulitic structure into a crystal array, in which molecules are forced into their most extended conformation (polar β phase), with all dipole moments aligned in the same direction. Furthermore, applying an electric field on both sides of the PVDF electrets (the electrical poling) also results in the orientation of the polar crystallite axis along the field direction, which promotes a higher spontaneous polarization for the β phase [10].

As a polymeric piezoelectric material in the form of an electrospun nanofibrous membrane, PVDF has been studied intensively [11–14] for components in flexible energy harvesting devices. However, it has been demonstrated that pure PVDF membranes' piezoelectric and mechanical properties are still insufficient for practical applications. There is thus a strong need for an enhancement of those properties of the membranes. A cost-effective approach is incorporating nanofillers with PVDF to produce new nanocomposites for synergistic structures and properties.

There is an agreement that the addition of MWCNTs facilitates PVDF transformation from α to β phase for electrospun PVDF/MWCNT nanocomposites [10, 15, 16]. The addition of MWCNT converts the α phase into β phase by acting as nuclei in the crystallization process and helping charge accumulation at the interface (facilitating the arrangement of PVDF chains in the β-phase conformation) [17]. In addition, interfacial electrostatic interaction between functional groups on MWCNTs and the CF_2 dipole of PVDF chains can make the PVF_2 chain more straightened, forming zigzag TTTT conformation of β phase instead of coiled TGTG′ conformation of α phase.

There is also an agreement that for electrospun PVDF/GO nanocomposites, graphene can act as a nucleating agent, providing a substrate for the formation of PVDF crystal nucleation and inducing β-phase formation of PVDF segment through strong interactions at the interface between PVDF dipole and graphene. The H atom of PVDF tended to be close to the graphene surface due to a high electronegativity C of sp^2 hybridization in graphene. In addition, conductive graphene could amplify the local electric field during in situ polarization and generate an induced charge, resulting in a stronger Coulomb force, which attracted the PVDF chain to crystallize into a β phase on the graphene surface [18, 19]. However, there is a lack of further study on piezoelectric properties correlated to the crystallinity data.

This work focuses on developing PVDF nanocomposite fibrous membranes via incorporating carbon nanofillers, including CNT and GO to enhance the piezoelectric performance of the nanocomposites. Nonwoven fibrous membranes of the PVDF/carbon composites were produced using the electrospinning process and characterized in terms of morphology, the total crystallinity of PVDF, the relative fraction of the β-phase PVDF, and piezoelectric property (d_{33}).

The formulation of PVDF/carbon suspensions was optimized through a systematic study on the effects of type and concentration of the carbon nanofillers and additives on the suspension stability for electrospinning. The electrospinning process conditions were established by optimizing the structure, morphologies, and corresponding piezoelectric properties of the nanocomposite fibrous membranes.

The correlation between β-phase volume fraction (piezoelectric phase) and piezoelectric property of the electrospun composite membranes was also analyzed.

2. Materials and Methods

All materials, unless specified, were supplied by Sigma-Aldrich. The average molecular weight (Mw) of PVDF is ~534,000 g/mol. The solvent used were N, N-Dimethylformamide (DMF) and a laboratory reagent grade acetone. Multiwalled carbon nanotubes (MWCNTs) supplied by Cambridge Nanosystems Ltd. have an average diameter of 60 ± 20 nm and an average length of 100-3000 μm, and purity and surface area of the MWCNTs are above 95% and 40 m^2/g, respectively. Graphene oxide (GO) was used in powder form (15-20 sheets, 4-10% edge-oxidized) with a density of ~1.8 g/cm^3.

Each batch of PVDF/CNT suspension prepared for electrospinning, as shown in Table 1, was approximately 5 mL, and a cosolvent used to dissolve PVDF was prepared from DMF and acetone with a volume ratio of about 20 : 11. A small quantity of polyvinylpyrrolidone (PVP, 4.8 wt.%) was

Table 1: Formulations of PVDF/carbon suspensions.

Sample ID	wt.% of carbon-based fillers	wt.% of PVDF	wt.% of acetone	wt.% of DMF	wt.% of PVP
CNT-0.01%	0.01	9.53	51.85	33.86	4.75
CNT-0.03%	0.03	9.52	51.84	33.86	4.75
CNT-0.05%	0.05	9.52	51.83	33.85	4.75
GO-0.5%	0.50	9.95	54.17	35.38	0
GO-1.5%	1.50	9.85	53.64	35.03	0
GO-2.5%	2.50	9.76	53.12	34.69	0

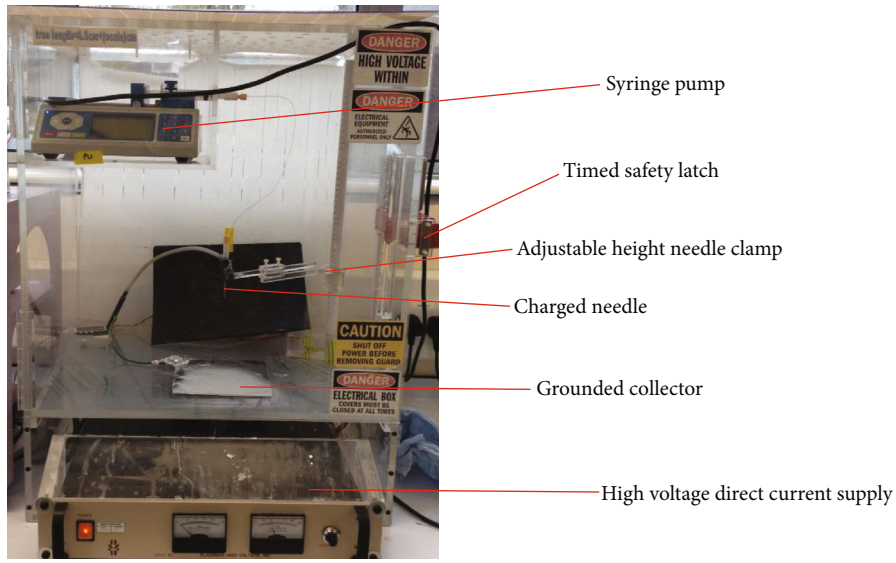

Figure 1: A purpose-built electrospinning device. The device comprises a syringe pump, charged needle, adjustable height needle clamp, grounded collector, high voltage direct current supply, and timed safety latch.

used as a dispersant to stabilize the suspensions. MWCNTs and PVP were first dispersed in the DMF/acetone cosolvent by sonicating the suspension with an ultrasonic probe (Branson Sonifier 250, UK) for 10 minutes to facilitate the uniform dispersion of MWCNT. PVDF was then dissolved in the MWCNT/PVP/DMF/acetone suspension and magnetically stirred for 20 minutes. As shown in Table 1, each batch of PVDF/GO suspension without PVP was prepared similarly. The GO powder was dispersed in DMF, and PVDF was dissolved in DMF/acetone separately and then mixed under magnetically stirring for 20 minutes.

The dispersion of the fillers (or destruction of the agglomerates) in the suspensions was assessed using optical microscopy. A droplet of suspension was sandwiched between two thin glass slides and then observed under a transmission light microscope (Zeiss Axioskop 2 MAT). Sedimentation tests were conducted to check if the stability of the suspensions was sufficient during the electrospinning process. The suspensions were placed into test tubes and checked each hour after preparation for signs of sedimentation (or phase separation) for up to 6 hours. The absence of obvious sedimentation over this length of time would be considered sufficiently stable for the duration of the electrospinning process, which typically lasts for less than an hour.

A purpose-built device, shown in Figure 1, was used for the electrospinning of the suspensions. It contains a Luer Lock syringe pump system fitted with a 14-gauge metal needle (1.70 mm inside diameter and 2.11 mm outside diameter) for dosing/delivering the suspensions at a flow rate of 1.0-1.6 mL/h. A voltage of 15-20 kV was applied between the tip of the needle and the flat-bed collecting plate separated by a distance of 150 mm. The collector plate was covered with aluminum foil to separate the plate's membranes easily. These electrospinning conditions are based on an experimental study to optimize parameters for the electrospinning of neat PVDF solutions. In addition, solid thin films made from neat PVDF solution and PVDF/carbon suspensions were prepared by casting the solution or the suspensions into a petri dish, and the solvent was evaporated in a fume cupboard overnight.

The morphology of the electrospun membranes was analyzed using a field emission scanning electron microscope (FESEM, Zeiss Supra 35VP) at 5 kV. The samples were coated with gold using a sputter coater before the examination.

For TEM observation, casting membranes made from the suspensions were embedded in epoxy resin and then sectioned into layers with a thickness of about 100 nm using

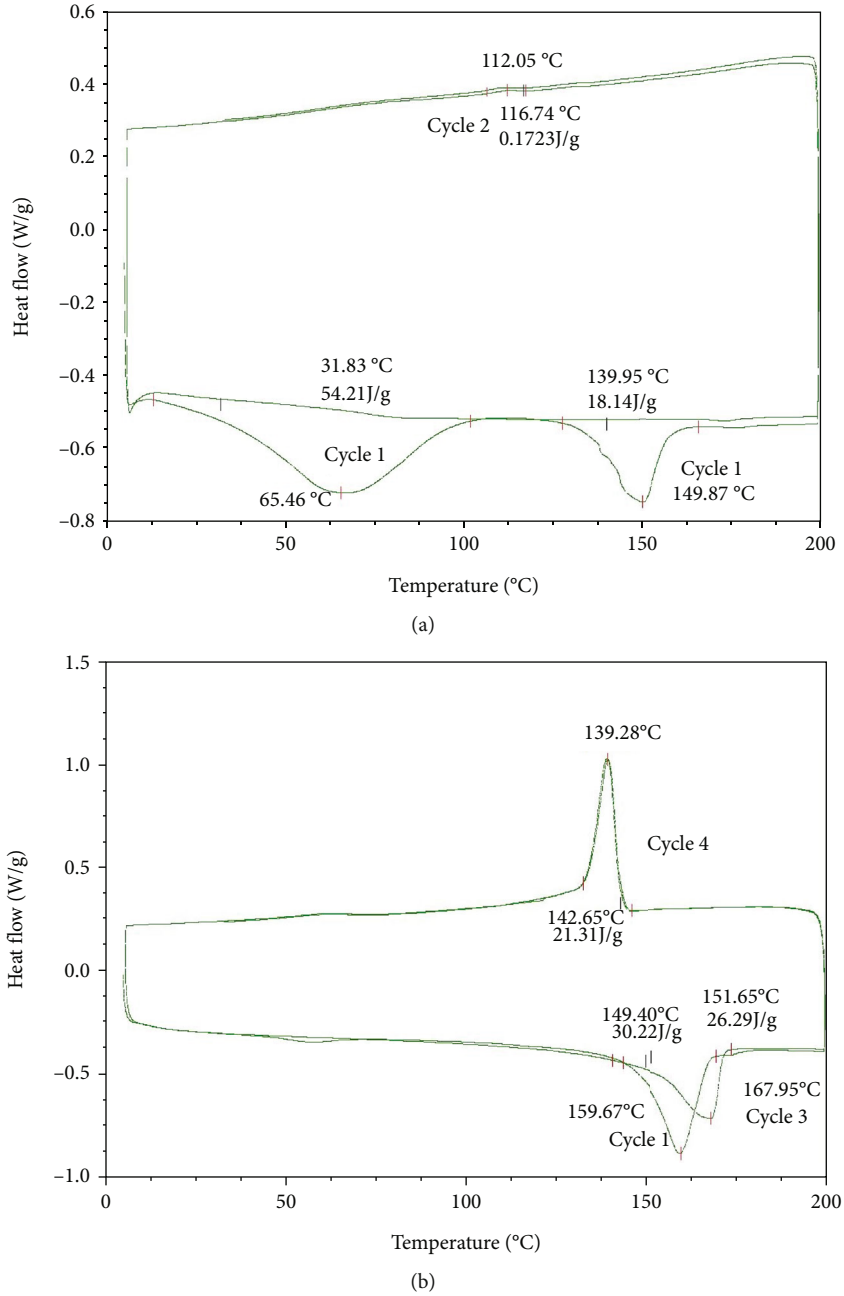

Figure 2: DSC patterns of (a) CNT-1.6% and (b) GO-4.6%. Each DSC test is composed of two "cycles," and the curve of the second cycle was used to calculate the heat of fusion.

RMC Boeckeler PT-PC Power Tome Ultramicrotomes. The sectioned samples were then placed on copper grids for TEM observation using a JEOL2100 field emission gun transmission electron microscope (FEG TEM). A range of areas of each sample were examined under TEM, and the most typical area was selected for presenting.

The total crystallinity of PVDF in the neat PVDF samples and PVDF/carbon nanocomposites were determined by a differential scanning calorimeter (DSC, TA Instruments, Q Series 2000) at a temperature scanning rate of 10°C/min in a nitrogen atmosphere. Each DSC test is composed of two "cycles" (in a sequence of heating-cooling-heating-cooling), and the curve of the second cycle was used to calculate the heat of fusion since the first cycle was used to eliminate the thermal history of the sample (see Figure 2).

The degree of crystallization in PVDF was approximately calculated from the endothermic peak of the melting of the composite fibers from the DSC dynamic heating curves using

$$X_c = \frac{\Delta H_m}{\Delta H_m^0} \times 100\%, \quad (1)$$

where X_c is the degree of crystallinity, ΔH_m is the heat of fusion (J/g) for the crystalline phases in PVDF, and $\Delta H_m{}^0$

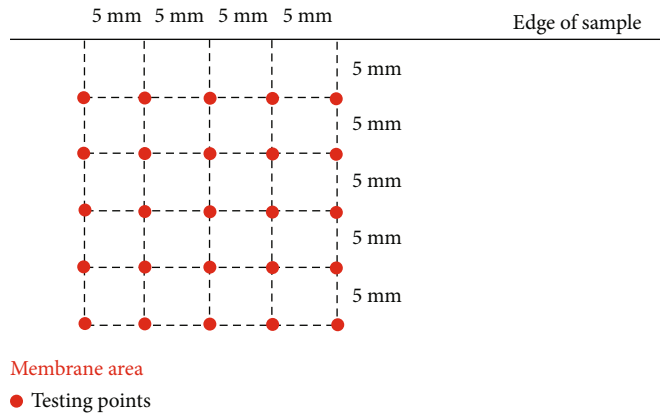

Figure 3: 5×5 points matrix for the d_{33} measurements. A 5×5 points matrix for the d_{33} measurements was used.

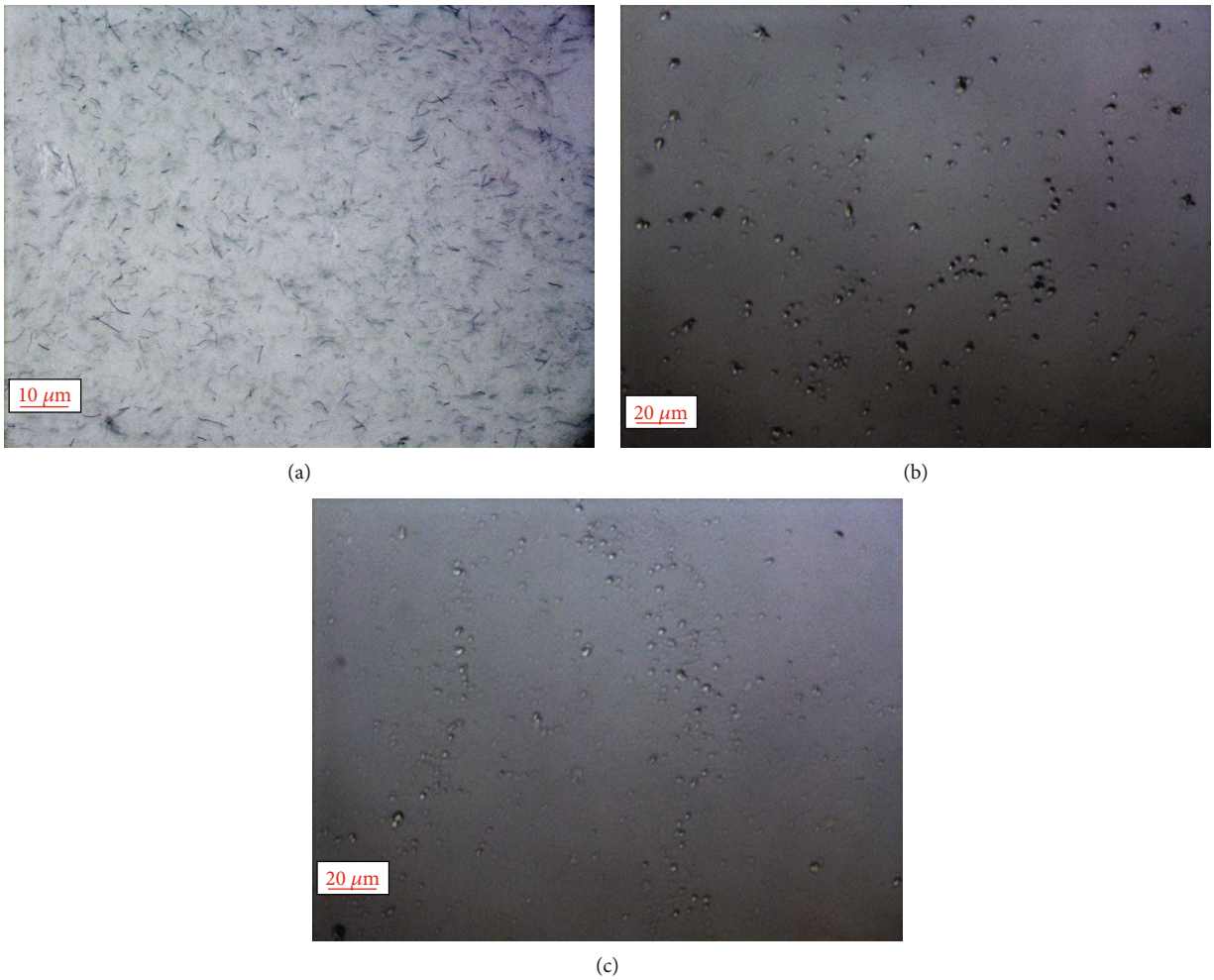

(a) (b)

(c)

Figure 4: Optical microscopic pictures of (a) CNT-0.01%, (b) CNT-0.03% and (c) CNT-0.05%.

is the heat of fusion for an imaginary case of 100% crystallinity which was calculated to be 104.6 J/g from the literature [20].

ΔH_m was obtained from the measured endothermic melting peak of DSC curves representing heat of fusion (J/g) for the composite, and $\Delta H_{m,s}$ was normalized by the PVDF content ω_P (wt.%) in the composites, which can be found in Table 1 using

$$\Delta H_m = \frac{\Delta H_{m,s}}{\omega_p}. \quad (2)$$

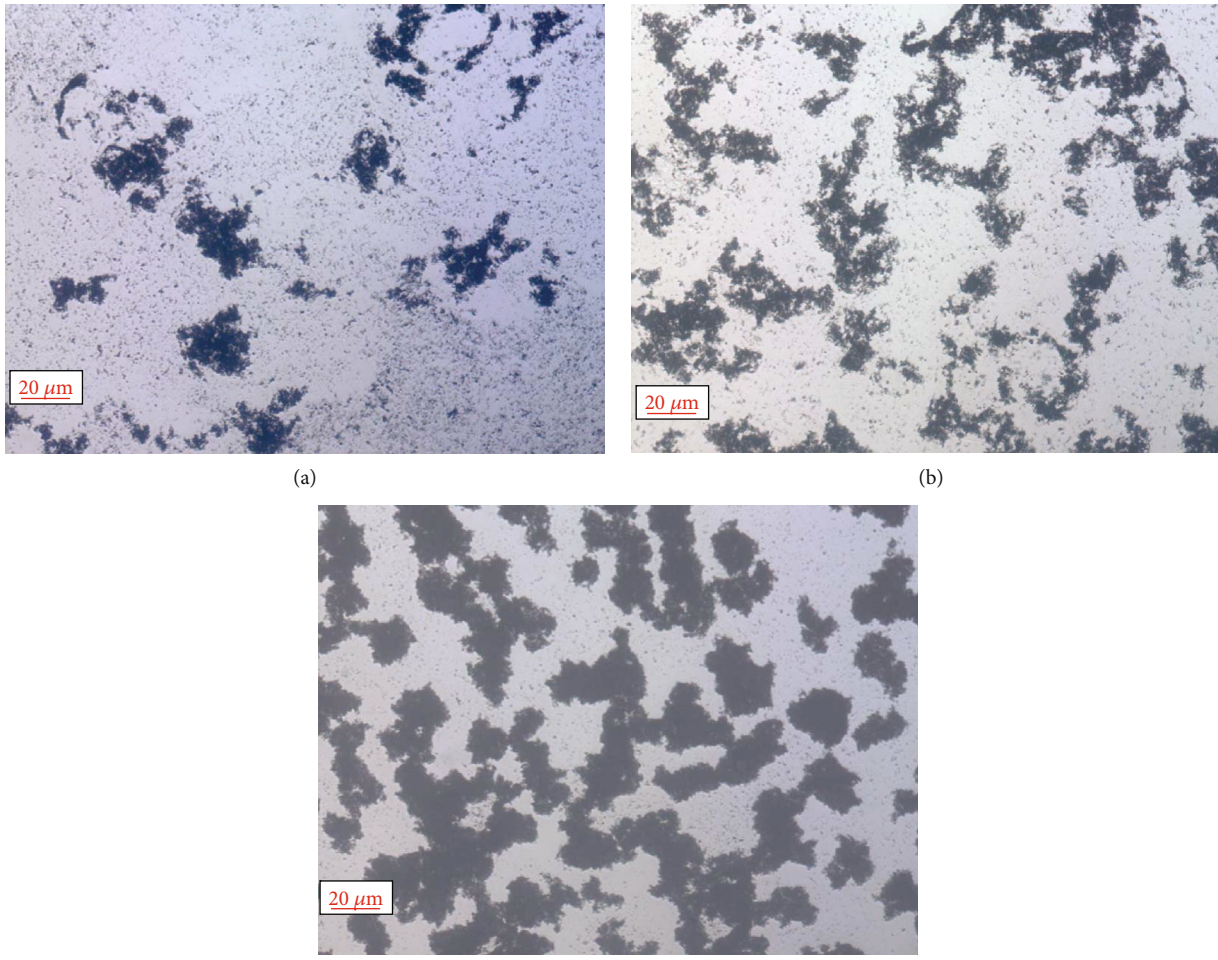

(a) (b)

(c)

Figure 5: Optical microscopic pictures of (a) GO-0.5%, (b) GO-1.5% and (c) GO-2.5%.

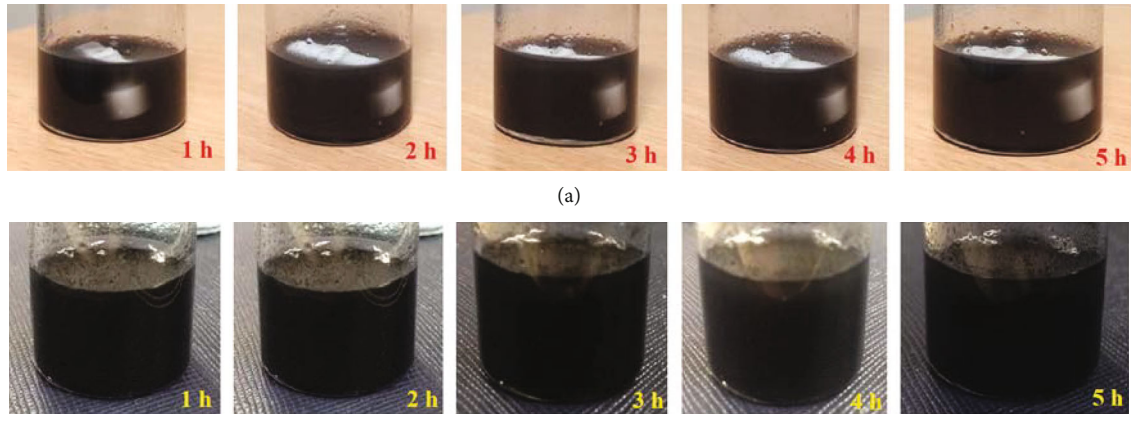

(a)

(b)

Figure 6: Sedimentation photo of (a) CNT-0.01% and (b) GO-0.5% suspensions after 1-5 hours. All the suspensions prepared were found to be sufficiently stable for the duration of the electrospinning process.

The Fourier transform infrared spectroscopy (FTIR) spectra of the nanocomposites were collected using a Perkin Elmer Spectrum One spectrometer. The as-received PVDF powder, electrospun membranes, and cast films were scanned from 4000 to 650 cm^{-1} in attenuated total reflectance mode (ATR). The relative fraction of the β phase (F_β) of the samples was quantified.

The piezoelectric charge constant d_{33} of electrospun nanocomposite membranes (with the aluminum foil on one side) was measured using a ZJ-6B d_{33}/d_{31} meter (Institute of

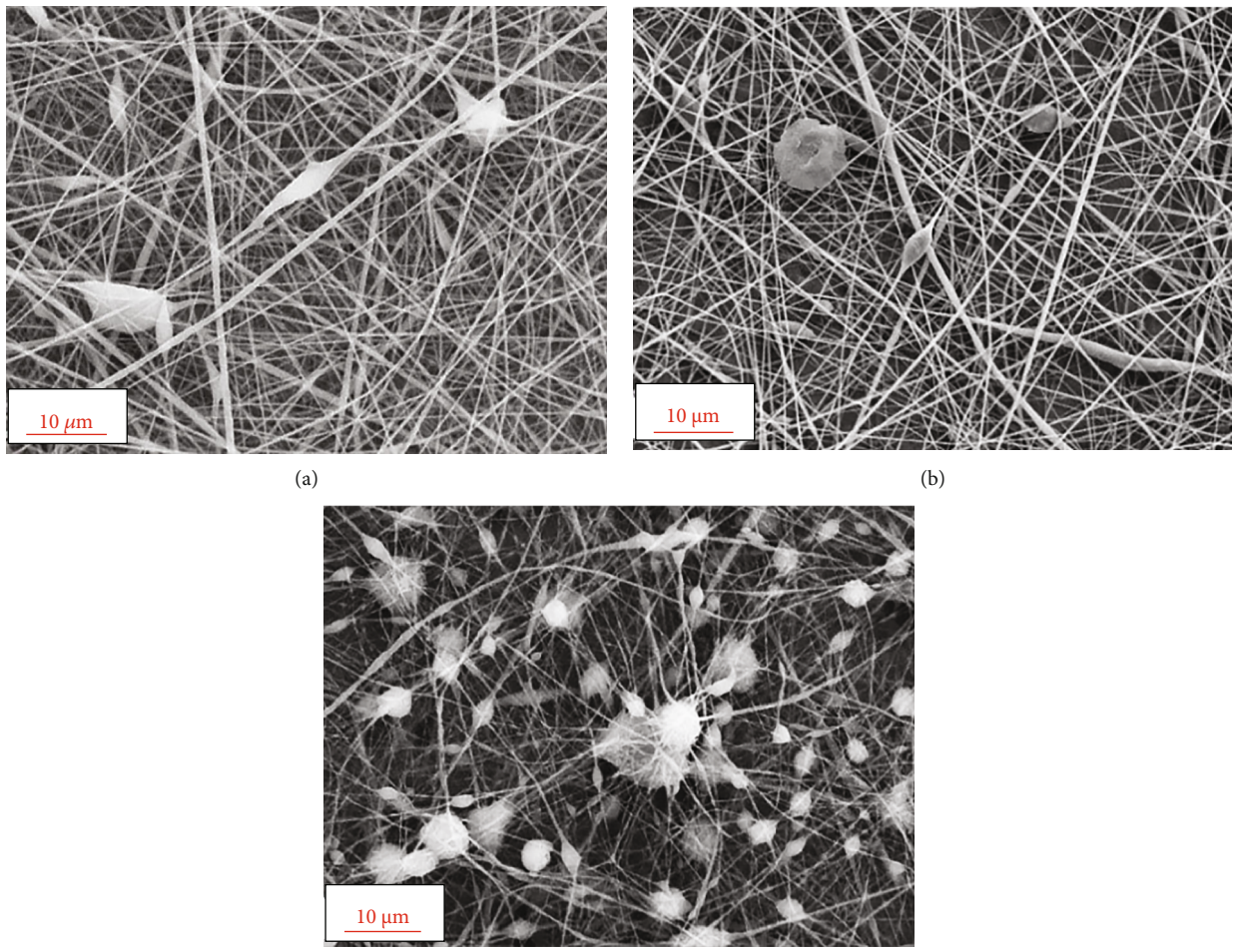

Figure 7: SEM microscopy showing the morphology and quality of electrospun membrane from suspensions: (a) CNT-0.01%, (b) CNT-0.03%, and (c) CNT-0.05%. As the loading of CNT increases, the population density of beads increases.

Acoustics, Chinese Academy of Sciences). A 5 × 5 points matrix for the d_{33} measurements was used, as shown in Figure 3. This matrix was designed to assess the variation of d_{33} over an area of measurement and to confirm if it is affected by the distance from the edge of the sample. 25 points across each sample, as shown in Figure 3, were tested. The d_{33} of electrospun nanocomposite membranes was calculated and averaged. d_{33} values of the membranes under different angle variations from their horizontal position (required by standard d_{33} measurement) were also measured to check if bending impacted the d_{33} values.

3. Results and Discussion

3.1. Dispersion/Sedimentation Stability of the Suspensions. The PVDF/PVP/CNT suspensions under the optical microscope (see Figure 4) showed that the CNT-0.01% was well dispersed without obvious agglomerates, but a certain amount of agglomerate residues could be observed in the CNT-0.03% and CNT-0.05% suspensions. This suggests that the ultrasonication method was not sufficiently powerful to completely break down the agglomerates within the as-received MWCNTs at higher concentrations.

PVP is a water-soluble, low-cost, nonionic polymer with C=O, C-N, and CH_2 functional groups and has been widely used to stabilize nanoparticles, which results from repulsive forces from its hydrophobic carbon chains [21]. PVP was added as a stabilizer for the PVDF/CNT suspensions but not for the PVDF/GO suspensions according to the needs based on preliminary observations on the stabilities of both suspensions.

In the PVDF/GO suspensions, well-distributed fine GO particles (see Figure 5) indicated that ultrasonication dispersed the as-received GO powder effectively. However, some loose clusters were found to increase in population with an increase in the GO loading. These are most likely to have resulted from flocculation of the originally dispersed particles, as observed by Song [22] due to insufficient interparticle repulsion in low-viscosity liquid systems, which the absorption of effective surfactants can minimize at suitable levels based on the loading of fillers [22].

No obvious sedimentation or phase separation was observed in any of the suspensions over the 5 hours after preparation (sedimentation tests of CNT-0.01% and GO-0.5% suspensions are shown in Figures 6(a) and 6(b)). Large and dense agglomerates tended to settle faster due to

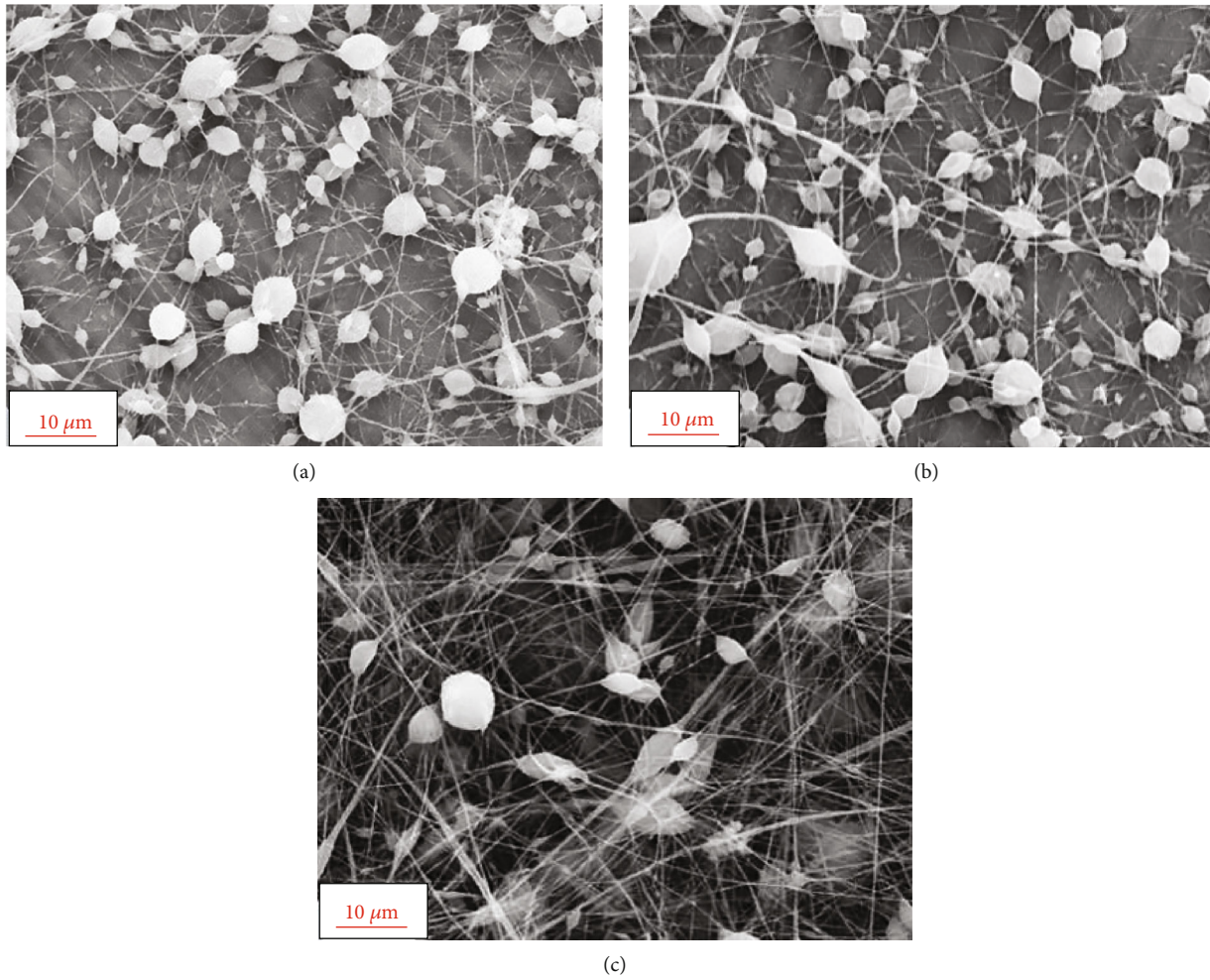

(a) (b) (c)

Figure 8: SEM microscopy shows the electrospun membrane morphology and quality from suspensions: (a) GO-0.5%, (b) GO-1.5%, and (c) GO-2.5%. Many beads and relatively fewer fibers were observed in GO-0.5% and GO-1.5%, while a decent nonwoven fibrous structure with a reduced number of beads was produced in GO-2.5%.

Table 2: The diameters of electrospun membrane nanofibers.

Sample ID	Range of diameter (nm)	Average diameter (nm)	SD (nm)
CNT-0.01%	370.27-1481.48	777.78	354.24
CNT-0.03%	370.37-1358.02	716.05	333.31
CNT-0.05%	370.17-864.20	604.94	169.18
GO-0.5%	349.65-699.30	475.52	113.24
GO-1.5%	576.92-961.54	673.08	135.98
GO-2.5%	392.16-1372.55	666.67	264.69

gravitation; the well-dispersed carbon fillers and smaller residual agglomerates show much more resistance to sedimentation. All the suspensions prepared were found to be sufficiently stable for the duration of the electrospinning process and did not cause any problem, such as clogging of the needle spinneret or the pipeline.

3.2. Morphology of the Electrospun Membranes. SEM microscope showing the morphology and quality of selective PVDF/CNT and PVDF/GO electrospun membranes is shown in Figures 7 and 8. The nanofibers of all the electrospun membranes have random orientations, but they can be aligned by using a rotating drum (disk) collector [23, 24].

For the PVDF/CNT system, as shown in Figure 7, as the loading of CNT increases, the population density of beads increases. This can be explained that bead generation is preferred at low-concentration polymer solution [25]; thus, higher polymer concentration is recommended to minimize the bead formation in the future works. Meanwhile, a certain amount of agglomerate residues was observed in the CNT-0.05% suspension. At the same time, CNT was well dispersed without obvious agglomerates in the CNT-0.01% suspension under the optical microscope, indicating that the agglomerates in the suspensions could have caused jet breakup during electrospinning, forming beads consequently. Therefore, the CNT-0.05% electrospun membrane has a much higher population density of beads than the CNT-0.01%. In general, the bead population density of the electrospun membranes increases with the agglomerate population density observed under optical microscopy (see Figure 4).

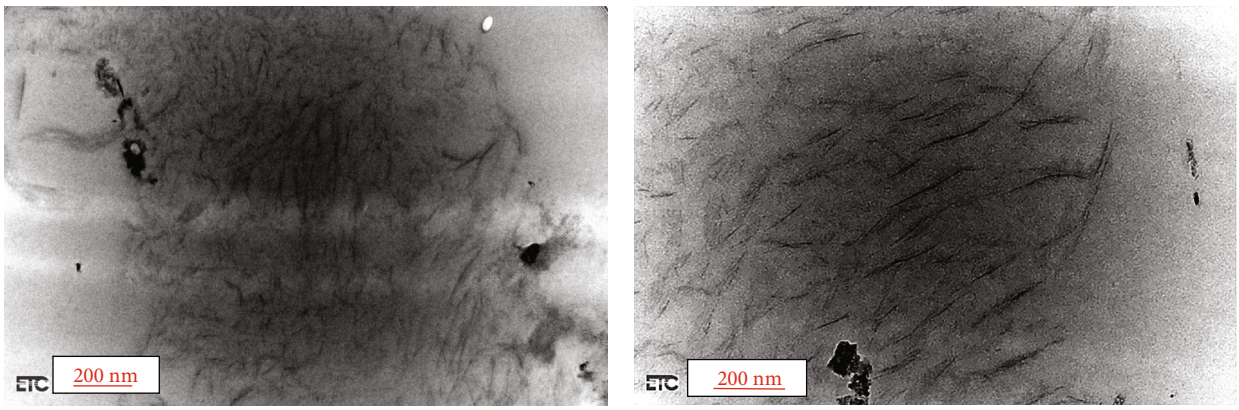

(a) (b)

Figure 9: TEM image of cross-section of the membrane cast from (a) CNT-0.03% to (b) CNT-0.05% suspensions. The MWCNTs or small nanotube bundles were well dispersed with a certain degree of orientation in the MWCNT composites.

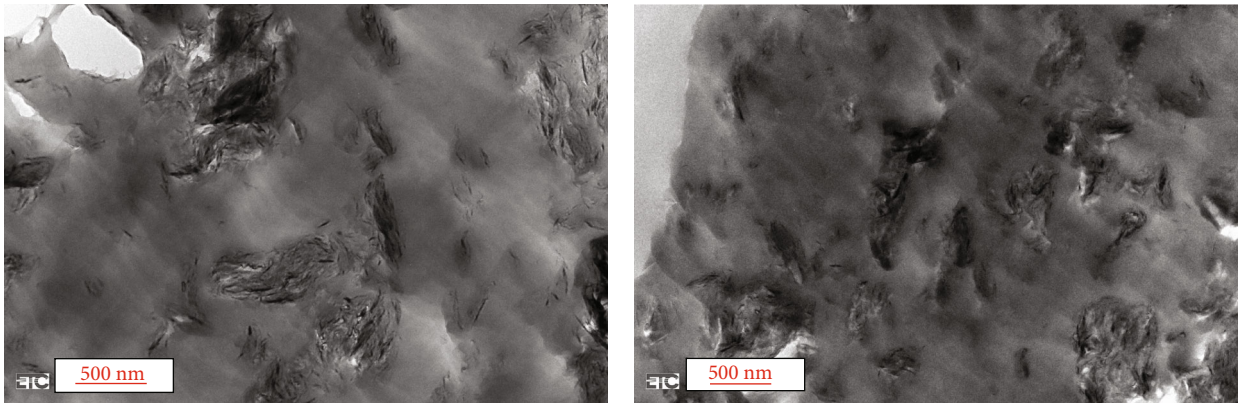

(a) (b)

Figure 10: TEM image of cross-section of the membrane cast from (a) GO-0.5% to (b) GO-1.5% suspension. Although some fine GO sheets were found, most are in loosely clustered form.

Table 3: $\Delta H_{m,s}$, ω_P, and X_c of PVDF in the electrospun membranes (the way of X_c calculation can be found in the "Materials and Methods" section).

Sample ID	$\Delta H_{m,s}$ (J/g)	ω_P (%)	X_c of PVDF (%)
Neat PVDF	48.9	100.0	46.7
CNT-0.01%	21.5	66.7	30.8
CNT-0.03%	21.3	66.6	30.5
CNT-0.05%	15.9	66.5	22.9
GO-0.5%	26.3	95.3	26.4
GO-1.5%	25.5	87.0	28.0
GO-2.5%	25.0	80.0	29.9

When electrospinning the PVDF/GO composites, as shown in Figure 8, a large number of beads and relatively fewer fibers were observed in GO-0.5% (Figure 8(a)) and GO-1.5% (Figure 8(b)), while a decent nonwoven fibrous structure with a reduced number of beads was produced in GO-2.5% (Figure 8(c)). The GO-2.5% suspension might possess higher charge density and dielectric constant than GO-0.5% and GO-1.5%, thus forming more fibers with less beads, which can be confirmed by examining charge density and dielectric constant of the suspensions in future work. Additionally, the particle flocculation in the GO suspensions could have caused jet breakup during electrospinning, forming beads consequently. Meanwhile, no clear correlation between the bead population density of the electrospun membranes and the agglomerate population density observed under optical microscopy (see Figure 5) can be observed. It is interesting to note that the beads are not isolated but connected by very fine fibers. This should be considered when considering electric conductivity and connectivity of the membrane, which can also be assessed in future work.

Uniform and beadless fibers are desirable in electrospun membranes. However, in practice, it is rather difficult to ensure 100% bead-free in membranes as both the

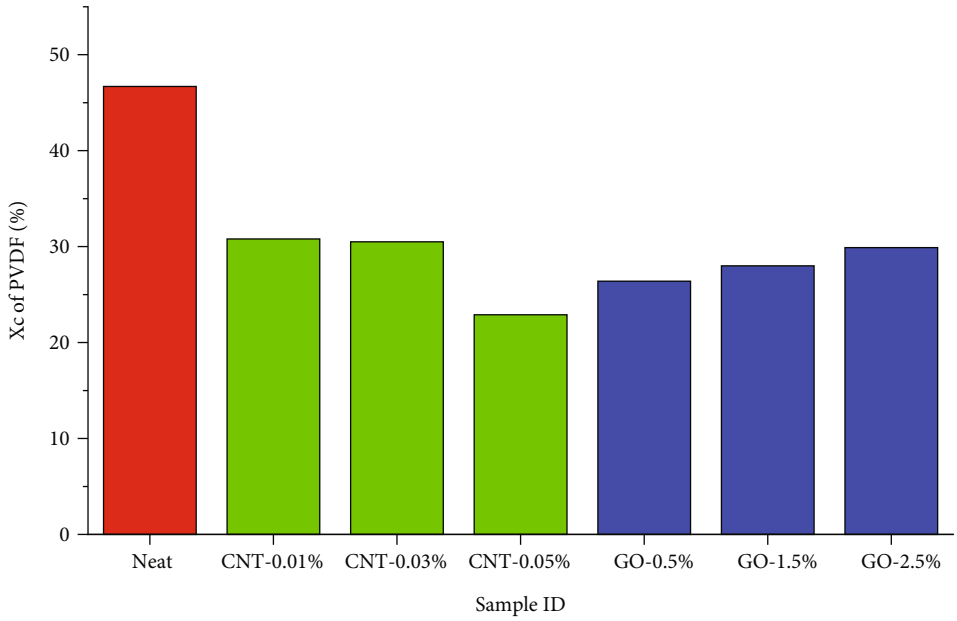

Figure 11: X_c of electrospun neat and PVDF/carbon nanocomposites fibrous membranes. The influence of carbon filler type and loading on X_c can be observed.

electrospinning conditions and suspension formulation may result in the formation of beads. The formation of beaded nanofibers can be considered a capillary breakup of electrospinning jets by surface tension, altered by the presence of electrical forces [26]. The viscoelasticity and surface tension of the solution, net charge density carried by jet, solution concentration, and the solvent dielectric constant are the major factors influencing bead formation [27].

Adequate viscosity is necessary to stabilize fiber against surface tension, which promotes bead formation. An increase in polymeric solute concentration enhances chain entanglements and thus the viscosity of solutions. Consequently, it helps to reduce the dominancy of the surface tension and results in fibers with fewer beads [28]. Therefore, bead generation is preferred at low-concentration polymer solution while higher concentrations lead to fiber formation (e.g., number of beads formed for CNT-0.05% compared to CNT-0.01% and CNT-0.03% shown in Figure 7) [25].

Fiber is formed by the stretching force created by electric potential, and thus high charge density favors the fiber formation. As the dielectric constant is a measure of the polarity of solvents, a solvent with high dielectric constant can induce a high net charge density on a solution, giving advantage for electrospinning fiber formation [27].

Additionally, future works can be further optimizing electrospinning process conditions, including liquid flow rate, voltage, and distance between the needle tip and the collector plate, and optimizing the solution viscosity and concentration, the jet net charge density, and the solvent dielectric constant, to minimize the bead formation for electrospun PVDF/carbon nanocomposites.

The diameters of electrospun membrane nanofibers were measured and summarized in Table 2, in which we can see that the average fiber diameter decreased and the diameter distribution narrowed with the loading of CNT increasing, while the average fiber diameter generally increased and the diameter distribution became wider with the loading of GO increasing. The influence of the fiber diameter on electrospun membrane can be studied in the future work.

3.3. Filler dispersion status of the nanocomposite fibrous membranes. The filler dispersion status of the nanocomposites was assessed by TEM. Figures 9 and 10 show the filler dispersion status in cross-section of electrospun membranes. As shown in Figure 9 for CNT-0.03% and CNT-0.05% nanocomposites, the MWCNTs or small nanotube bundles were well dispersed with a certain degree of orientation in the MWCNT composites.

The filler dispersion status in cross-section of the membrane cast from GO-0.5% to GO-1.5% suspensions was examined by TEM, as shown in Figure 10. Although some fine GO sheets (single- and a few-layered graphene) were found, most of them are in loosely clustered form, which agrees with optical microscope observations. Such loose packing allowed for the penetration of the PVDF polymer matrix, resulting in intercalated layered structures predominated within the PVDF matrix.

3.4. PVDF Crystallinity in the PVDF/Carbon Nanocomposites Fibers. The PVDF crystallinities of electrospun PVDF/CNT and PVDF/GO composite nanofibers were determined by DSC (see the "Materials and Methods" section).

The crystallinity of each electrospun composite nanofibers is listed in Table 3 and plotted in Figure 11. In comparison with the electrospun neat PVDF, the influence of the different carbon-based fillers (and their loading) on the total PVDF crystallinity (X_c) was revealed. Overall, the inclusion

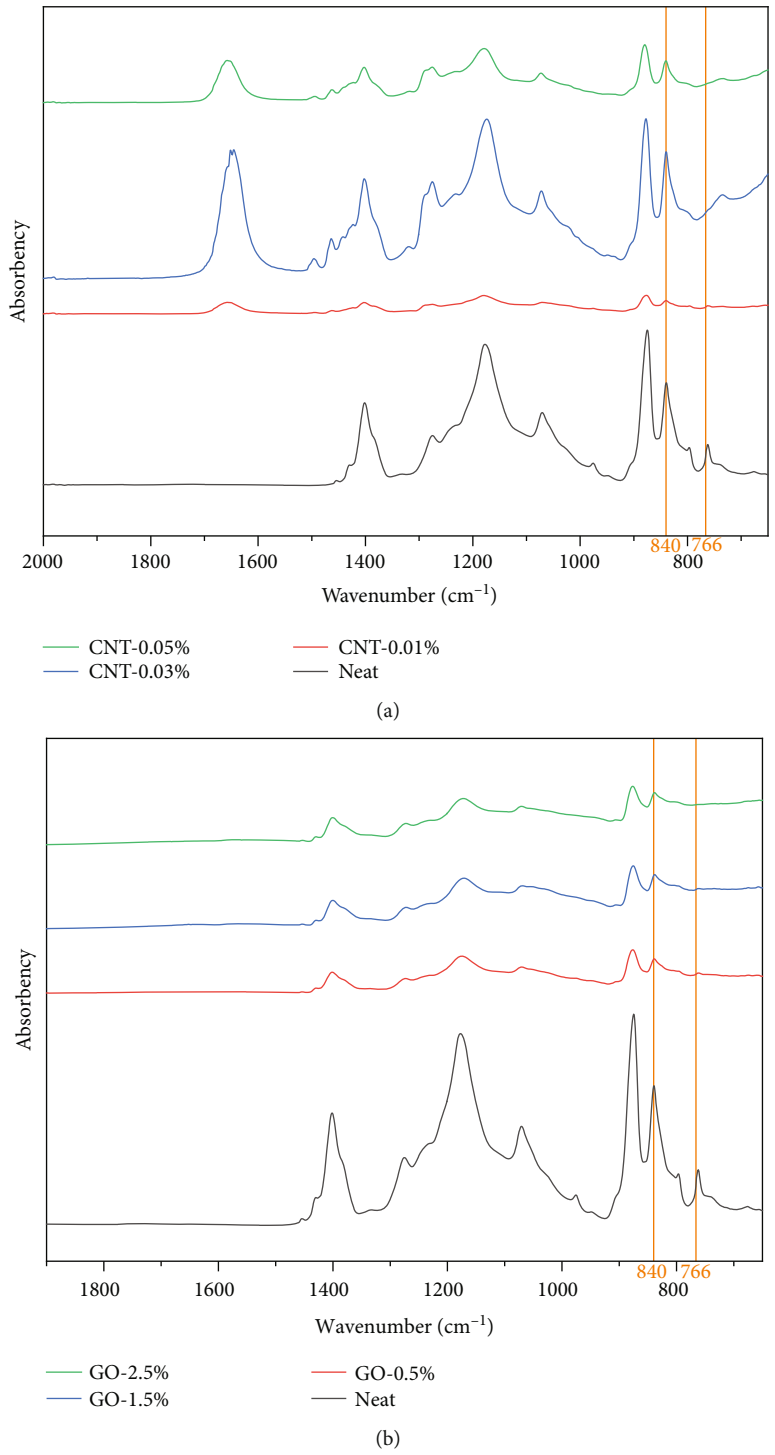

Figure 12: FTIR spectra of (a) PVDF/CNT composites and (b) PVDF/GO composites. The characteristic peak of the α phase and β phase is at 766 cm^{-1} and 840 cm^{-1}, respectively (as labeled).

of all types of carbon-based fillers had resulted in a considerable reduction of X_c, and X_c decreased with the CNT loading in the PVDF/CNT system while increased with the GO loading in the PVDF/GO system. Baji et al. observed a similar phenomenon and argued that MWCNTs could constrain molecular mobility in amorphous regions of PVDF during electrospinning, giving rise to the hindrance of PVDF crystallization (reduction of X_c) [29]. Wu and Chou found that MWCNTs restricting motions of molecules is due to a strong physical interaction between CNT and PVDF molecular chains [16], which can also be applied for the PVDF/GO composites. Additionally, GO particles' flocculation

Table 4: F_β of electrospun membranes (the way of F_β calculation can be found earlier in this section).

Sample ID	F_β (%)
Neat PVDF	72.0
CNT-0.01%	58.3
CNT-0.03%	59.6
CNT-0.05%	62.1
GO-0.5%	54.0
GO-1.5%	48.7
GO-2.5%	47.7

and the resulting intercalated structure may have restricted nucleation and growth of PVDF crystals in the confined spaces between the GO layers.

3.5. Relative Fraction of β Phase, F_β, in PVDF/Carbon Nanocomposite Fibers. PVDF is commonly crystallized in the nonpolar crystalline α phase, but it is the β phase that possesses piezoelectric property [30]. It follows that it should be the fraction of the β phase, not the total crystallinity X_c (see Section 3.5), that should be characterized and correlated to the piezoelectric properties of the composites. FTIR data (Figure 12) confirmed that α and β phases were predominant phases [31], and other phases are negligible, therefore, allowing to estimate the fraction of β phase in the total crystallinity. The relative fraction of β phase, F_β, in the total crystalline phases of PVDF was obtained from the FTIR spectra of the as-received PVDF powder, the electrospun membranes, and cast films using Equation (3) based on the assumption that infrared absorption follows the Lambert-Beer law [30].

$$F_\beta = \frac{A_\beta}{1.26A_\alpha + A_\beta} \times 100\%, \tag{3}$$

where A_α is the absorbency by α phase at 766 cm^{-1}(skeletal bending and CF_2 bending, where the characteristic peak of α phase is) and A_β is the absorbency by β phase at 840 cm^{-1} (CH_2 rocking, where the characteristic peak of β phase is). Repeatability of the F_β calculation was assessed using multiple FTIR scans for a given sample, and the discrepancy was found to be negligible (standard deviation in F_β was found to be 0.014%), and thus, a single scan was considered sufficient for the calculation of F_β for each sample. F_β for the neat PVDF electrospun membrane and electrospun PVDF/carbon composites are listed in Table 4 and plotted in Figure 12.

F_β for the as-received PVDF powder and the electrospun neat PVDF is 55.1% and 72.0%, respectively, indicating that the electrospinning process promoted the formation of β-crystalline phase, as reported elsewhere [12–14].

The influence of loading on F_β in Table 4 and Figure 13 varied with filler types. For both the PVDF/CNT and the PVDF/GO systems, the addition of CNT and GO resulted in an overall reduction of F_β in comparison with the neat PVDF. F_β increased with the increase of CNT loading while decreasing with the GO loading. F_β increasing with the increase of CNT loading agrees with many studies that the addition of MWCNTs facilitates PVDF transformation from α to β phase [10, 15, 16], by acting as nuclei in crystallization and helping charge accumulation at the interface, arranging PVDF chains in the β-phase conformation, because the interfacial electrostatic interaction between the functional groups on MWCNTs and the CF_2 dipole of PVDF chains can make PVF_2 chain more straightened [17]. The decreasing F_β value with increasing loading of the GO particles indicates that there is an optimum GO particle concentration to obtain a well-developed β-crystalline phase in PVDF/GO composites; the optimum concentration is 0.1 wt.% [32] which is lower than the loading of GO in this study (0.5-2.5 wt.%), while after exceeding the optimum concentration, the higher the concentration, the greater negative effect on F_β from the addition of GO.

3.6. Volume Fraction of β Phase in the PVDF and PVDF/Carbon Composites. Some studies [33–36] speculated that the improvement in piezoelectric property of PVDF composites was simply based on the increase of relative fraction, F_β. However, it seems more reasonable that since it is the β phase that possesses the piezoelectric property in PVDF, piezoelectric performance of the PVDF composite should depend on the volume fraction of the β phase in the composites rather than the relative fraction F_β in the crystalline PVDF. The β-phase volume fraction, v_β, can be calculated using Equations (4) and (5) (as mentioned in the "Relative fraction of β phase, F_β, in PVDF/carbon nanocomposite fibers" section, α and β phases were predominant phases and other phases were negligible):

$$v_\beta = \frac{m_\beta/\rho_\beta}{\left(m_f/\rho_f\right) + \left(m_A/\rho_A\right) + \left(m_\alpha/\rho_\alpha\right) + \left(m_\beta/\rho_\beta\right)}, \tag{4}$$

$$m_\beta = m_s \times \omega_P \times X_c \times F_\beta, \tag{5}$$

where v_β is the volume fraction (vol.%) of β-phase PVDF in neat PVDF samples and PVDF/carbon composites; m_s, m_f, m_A, m_α, and m_β (calculated by using Equation (5)) are the mass of the sample, filler, amorphous PVDF, α-phase PVDF, and β-phase PVDF, respectively; ρ_β, ρ_A, ρ_α, and ρ_f are the densities of the β, α, and amorphous phases in PVDF and that of the fillers (as listed in Table 5); ω_P is the mass fraction (wt.%) of PVDF on a dry basis in the samples, while X_c and F_β are as defined earlier. The volume fraction of the β phase in the samples, v_β, is listed in Table 6 and plotted in Figure 14.

As shown in Table 6 or Figure 14, the volume fraction of β phase in the samples, v_β for electrospun neat PVDF, is much higher in general than that of the as-received PVDF and the PVDF/carbon composites. It is clear that the electrospinning process promotes the formation of the β phase, as mentioned earlier, but the addition of CNT and GO

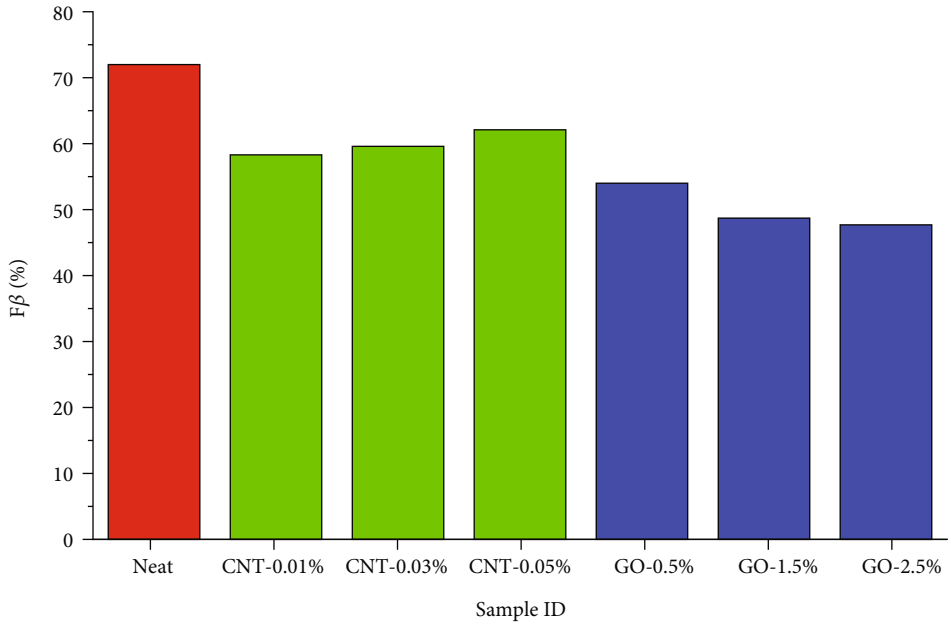

Figure 13: F_β of electrospun neat and PVDF/carbon nanocomposites fibrous membranes. The influence of carbon filler type and loading on F_β can be observed.

Table 5: Densities of different PVDF phases and carbon-based fillers.

PVDF phases/fillers	Density (g/cm^3)
Amorphous-PVDF	1.68
α-PVDF	1.92
β-PVDF [37]	1.97
CNT [38]	2.00
GO [39]	1.80

Table 6: Volume fraction of β phase, v_β, in the PVDF and PVDF/carbon composites (the way of v_β calculation can be found earlier in this section).

Sample ID	v_β (vol.%)
The as-received PVDF	18.15
Neat PVDF	30.70
CNT-0.01%	15.98
CNT-0.03%	16.14
CNT-0.05%	12.47
GO-0.5%	12.03
GO-1.5%	10.56
GO-2.5%	10.20

significantly hindered the β-phase formation. In addition, v_β decreased with increasing the loading of CNT and GO in general. The reason why F_β increased but v_β decreased with the increase of CNT loading is as follows: when the CNT loading increases, the m_f in the Equation (4) increases, while it is difficult to tell whether m_β increases or decreases (according to Equation (5), m_β is decided by m_s, ω_P, X_c, and F_β, and when CNT loading increases, m_s increases, ω_P decreases, X_c decreases, and F_β increases) but changes with the same trend on both numerator and denominator of the Equation (4), in which other factors do not change with CNT loading; therefore, with m_f increases, the result of Equation (4) (v_β) decreases with the increase of CNT loading. Since the calculation of v_β has considered the combined influence of fillers on X_c and F_β, both of which were reduced by incorporating CNT and GO; therefore, v_β was expected to decrease. In addition, the v_β of the PVDF/CNT composites were higher than that of the PVDF/GO composites, while the loadings of GO are much higher than CNT. Therefore, it would be logical to anticipate that the piezoelectric property of the materials of interest would follow the ranking: neat electrospun PVDF, the as-received PVDF, the PVDF/CNT, and the PVDF/GO composites, and this will be discussed together with the d_{33} data. Presume from the previous discussions that the inclusion of carbon-based fillers is not beneficial for enhancing piezoelectric property. However, it is worth noting that although v_β is assumed to be a key factor that determines piezoelectric property, other factors such as the crystalline orientation and the composites' electric conductivity can also play a part.

3.7. Piezoelectric Properties. Piezoelectric coefficient d_{33} values were directly measured by the ZJ-6B d_{33}/d_{31} meter.

The influence of the distance between the measurement points and the edge and the angle variation from their horizontal position (required by standard d_{33} measurement) is shown in Table 7, where the mean piezoelectric coefficient d_{33} was obtained from the average of 5 points of the same

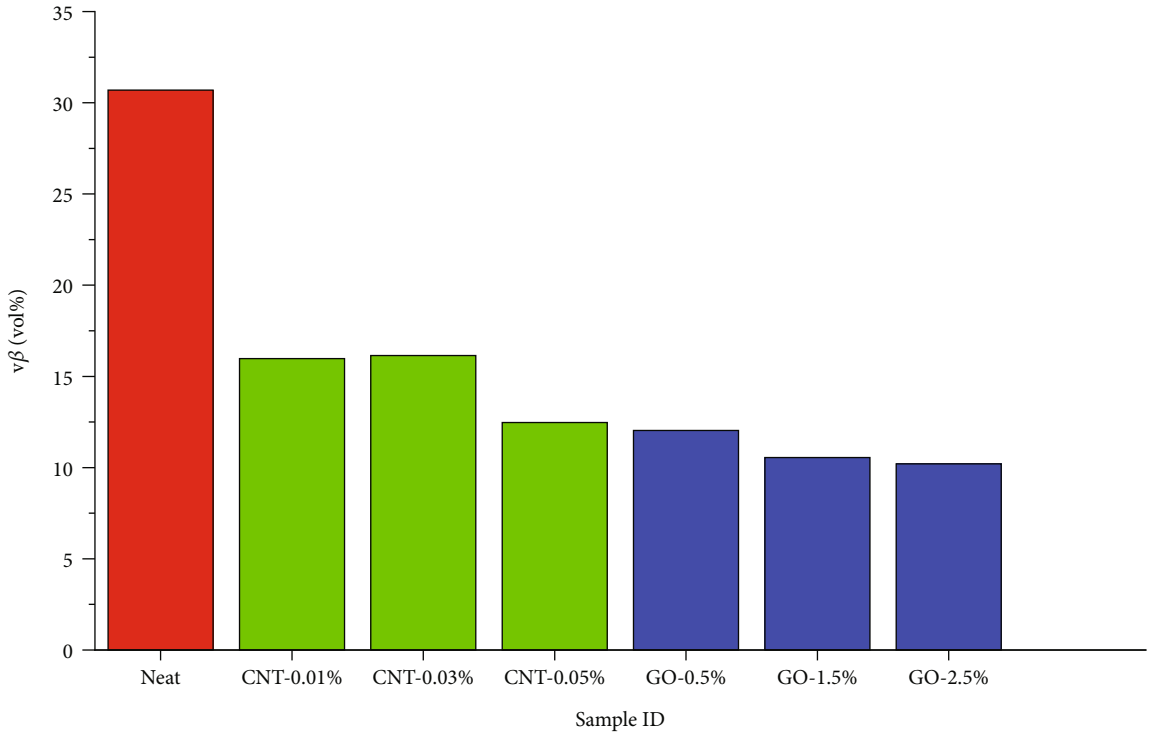

Figure 14: Volume fraction of β phase, v_β, in the PVDF and PVDF/carbon composites. The influence of carbon filler type and loading on v_β can be observed.

Table 7: d_{33} measurement showing the influence of distances to the edge of sample and angle from the horizontal position for CNT-0.01%.

Distance/angle	d_{33} (pC/N)	SD (pC/N)
5 mm	12.00	±1.22
10 mm	14.40	±3.05
15 mm	12.20	±2.17
20 mm	14.00	±2.45
25 mm	14.80	±1.79
12°	11.60	±1.52
24°	10.80	±1.64
36°	11.00	±1.58
48°	10.80	±0.84
60°	11.00	±1.41

distance from the edge. As all the selected samples show the same trend, only one is presented here.

Table 7 shows that the d_{33} for the same distance is consistent (low standard deviations). No systematic variations can be found as a function of the distance, and thus, the influence of choices of measurement position points can be neglected. However, a noticeable overall reduction of d_{33} values can be observed when the membranes deviated from the required horizontal position, most likely due to additional stress generated from the bending. Thus, care must be taken to avoid such bending to minimize measurement errors.

Table 8: Results of the d_{33} measurement for electrospun neat PVDF and the PVDF/carbon composite membranes comparing with other commonly used piezoelectric materials (the way of X_c calculation can be found in the "Materials and Methods" section and earlier in this section).

Sample ID	d_{33} (pC/N)	SD (pC/N)
Neat PVDF	10.00	±0.71
CNT-0.01%	13.58	±2.19
CNT-0.03%	15.97	±1.85
CNT-0.05%	13.61	±1.15
GO-0.5%	10.50	±1.52
GO-1.5%	8.67	±0.75
GO-2.5%	7.46	±2.59
Quartz crystal [41]	2-3	—
AlN [41]	5	—
ZnO [41]	12.4	—
P(VDF-TrFE) [41]	20	—
$BaTiO_3$ [40]	190	—
PZT [41]	225-593	—

Using the $5 \times 5 d_{33}$ measurement point matrix, the mean d_{33} was obtained from averaging the 25 points. The results are summarized in Table 8 (comparing with other commonly used piezoelectric materials [40, 41]) and plotted in Figure 15.

It is clear from Table 8 and Figure 15 that the d_{33} for the electrospun neat PVDF (10 pC/N) can be succeeded by that

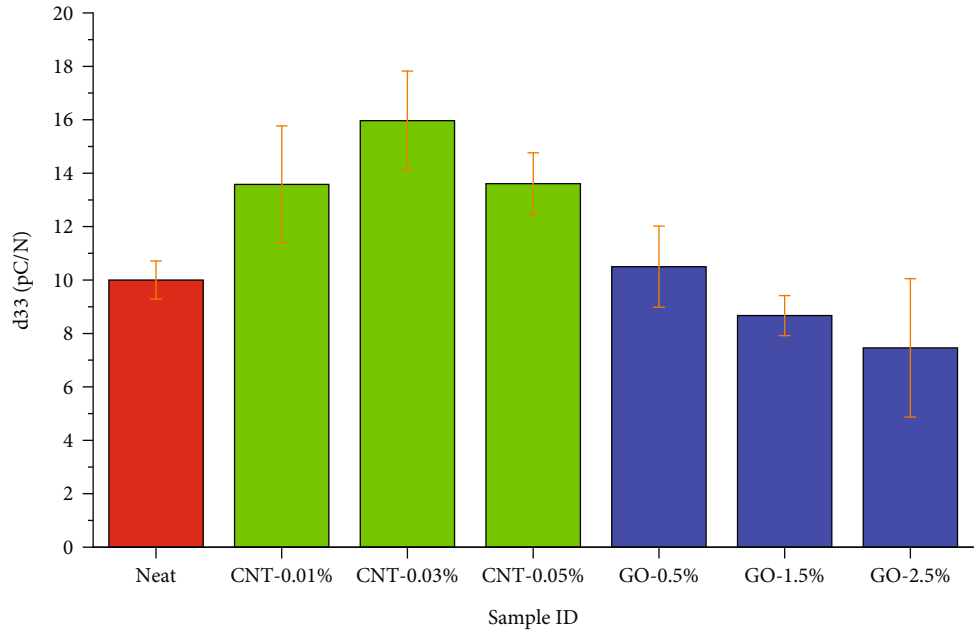

FIGURE 15: Results of the d_{33} measurement for electrospun neat PVDF and PVDF/carbon composite membranes. The influence of carbon filler type and loading on d_{33} can be observed. The error bars represent the standard deviation of 25 measurements ($n = 25$).

of both PVDF/CNT and PVDF/GO composites at certain loadings.

In the PVDF/CNT system, CNT loadings higher than 0.01 wt.% are sufficient to outperform the neat PVDF and become 59.7% higher than that d_{33} of the neat PVDF at a 0.03 wt.% CNT loading. Similar results have been reported by Pu et al. [12]. As shown in Table 6 and Table 8, v_β decreased by 47.43-59.38%, while d_{33} increased by 35.8-59.7% when 0.01-0.05 wt.% CNT was added. The d_{33} increase in the PVDF/CNT system may have been caused by the increased electrical conductivity by CNT due to its high electric conductivity [23, 42] and by possibly the enhanced orientation of β crystals. The former would conduct the charge of the polycrystalline β phase to the surface of the membrane, and the latter would enhance the coordinated response from the β-phase polycrystalline in the d_{33} direction. The orientation of the β crystals can be promoted by increased electrostatic force during electrospinning owing to the enhanced electrical conductivity of PVDF solution by CNT. Additionally, Wu and Chou found that the addition of CNTs into the piezoelectric polymer can improve piezoelectricity through interfacial polarization [16]. Mobile charges within conductive CNTs can facilitate composite polarization; thus, interfacial polarization increases the dielectric constant of the composite.

In the PVDF/GO system, only GO loadings of 0.5 wt.% achieved a d_{33} comparable to the neat PVDF. Further increasing in GO loading had resulted in a declined d_{33}. In general, d_{33} of the PVDF/CNT composites is higher than that of the PVDF/GO composites. This may be due to the high conductivity of pristine MWCNTs, which may improve electron transfer within the composites. On the other hand, despite much higher loading of GO and low conductivity of GO [41], influence of flocculation and the lower aspect ratio compared with CNT [43] may result in lower electron transfer and less orientation of the β-phase polycrystalline.

4. Conclusions

Electrospun PVDF/CNT and PVDF/GO nanocomposites with different loadings were manufactured by the electrospinning process, and the influence of fillers on the crystalline and piezoelectric properties was studied, which can be summarized as the following points:

(i) The inclusion of carbon fillers considerably reduced the total PVDF crystallinity (X_c) comparing with the neat electrospun PVDF (by 34.05-50.96%)

(ii) The X_c decreased with the CNT loading while increased with the GO loading

(iii) The PVDF crystallization hindrance is due to the molecular mobility restriction, strong physical interaction between fillers and PVDF molecular chains, and the GO particles' flocculation and the intercalated structure

(iv) The inclusion of carbon fillers reduced the relative fraction of β phase in the total crystalline PVDF (F_β) comparing with the neat PVDF (by 19.03-33.75%)

(v) The F_β increased with CNT loading while decreased with GO loading

(vi) CNT can facilitate PVDF α- to β-phase transformation by acting as nuclei and helping interface charge accumulation

(vii) The negative effect from the GO on the F_β grows with the GO concentration while exceeding the optimum concentration for β-phase (0.1 wt.%)

(viii) The inclusion of carbon fillers considerably reduced the volume fraction of the β phase (v_β) comparing with the neat electrospun PVDF (by 47.43-59.38%)

(ix) v_β generally decreases with carbon filler loading increases

(x) Since the calculation of v_β has considered the combined influence of fillers on X_c and F_β, both of which were reduced by filler inclusion, leading to v_β reduction

(xi) The v_β of the PVDF/CNT composites were higher than the PVDF/GO composites, though the CNT loading was much lower than the GO loading

(xii) The piezoelectric coefficient d_{33} for the electrospun neat PVDF is 10 pC/N, which can be succeeded by PVDF/CNT and PVDF/GO composites at certain loadings

(xiii) d_{33} of samples with CNT loadings higher than 0.01 wt.% outperformed the neat PVDF and became 59.7% higher than the d_{33} of the neat PVDF at 0.03 wt.% loading (d_{33} increased by 35.8-59.7% when 0.01-0.05 wt.% CNT was added)

(xiv) The d_{33} increase in the PVDF/CNT system may be caused by the increased electrical conductivity by CNT, the enhanced β crystals' orientation, and improved composite piezoelectricity by CNT through interfacial polarization increasing the dielectric constant

(xv) For PVDF/GO system, only GO loading of 0.5 wt.% achieved comparable d_{33} to the neat PVDF; further increase in loading had resulted in a decline in d_{33}

(xvi) The d_{33} of the PVDF/CNT composites is higher than that of the PVDF/GO composites, despite much higher loading of GO, low conductivity of GO, and influence of flocculation, and the lower aspect ratio compared with CNT may result in lower electron transfer and less β crystals' orientation

Future works suggested:

(i) Further optimizing electrospinning process conditions, solution viscosity and concentration, the jet net charge density, and the solvent dielectric constant, to minimize the bead formation for electrospun PVDF/carbon nanocomposites

(ii) Electrical conductivities of the PVDF/carbon suspensions and electrospun membranes can be examined to prove the analyses in this study

(iii) β crystals' orientation of the PVDF/carbon electrospun membranes can be examined to prove the analyses in this study

Data Availability

Data is available upon request.

Conflicts of Interest

The authors declare that there is no conflict of interest regarding the publication of this paper.

References

[1] H. Kawai, "The piezoelectricity of poly (vinylidene fluoride)," *Japanese Journal of Applied Physics*, vol. 8, no. 7, pp. 975-976, 1969.

[2] E. Erdtman, K. C. Satyanarayana, and K. Bolton, "Simulation of α- and β-PVDF melting mechanisms," *Polymer (Guilford)*, vol. 53, no. 14, pp. 2919–2926, 2012.

[3] J. R. Gregorio and M. Cestari, "Effect of crystallization temperature on the crystalline phase content and morphology of poly(vinylidene fluoride)," *Journal of Polymer Science Part B: Polymer Physics*, vol. 32, no. 5, pp. 859–870, 1994.

[4] K. Tashiro, "Crystal structure and phase transition of PVDF and related copolymers," *Plastics Engineering-New York*, vol. 28, p. 63, 1995.

[5] J. Gomes, J. Serrado Nunes, V. Sencadas, and S. Lanceros-Mendez, "Influence of the β-phase content and degree of crystallinity on the piezo- and ferroelectric properties of poly(vinylidene fluoride)," *Smart Materials and Structures*, vol. 19, no. 6, article 065010, 2010.

[6] S. M. Hosseini and A. A. Yousefi, "Piezoelectric sensor based on electrospun PVDF-MWCNT-Cloisite 30B hybrid nanocomposites," *Organic Electronics*, vol. 50, pp. 121–129, 2017.

[7] X. Liu, Y. Shang, J. Zhang, and C. Zhang, "Ionic liquid-assisted 3D printing of self-polarized β-PVDF for flexible piezoelectric energy harvesting," *ACS Applied Materials & Interfaces*, vol. 13, no. 12, pp. 14334–14341, 2021.

[8] E. K. Akdogan, M. Allahverdi, and A. Safari, "Piezoelectric composites for sensor and actuator applications," *IEEE Transactions on Ultrasonics, Ferroelectrics, and Frequency Control*, vol. 52, no. 5, pp. 746–775, 2005.

[9] F. L. Zhou and R. H. Gong, "Manufacturing technologies of polymeric nanofibres and nanofibre yarns," *Polymer International*, vol. 57, no. 6, pp. 837–845, 2008.

[10] Y. Ahn, J. Y. Lim, S. M. Hong et al., "Enhanced piezoelectric properties of electrospun poly (vinylidene fluoride)/multiwalled carbon nanotube composites due to high β-phase formation in poly (vinylidene fluoride)," *The Journal of Physical Chemistry C*, vol. 117, no. 22, pp. 11791–11799, 2013.

[11] N. Chanunpanich and H. Byun, "Alignment of electrospun polystyrene with an electric field," *Journal of Applied Polymer Science*, vol. 106, no. 6, pp. 3648–3652, 2007.

[12] J. Pu, X. Yan, Y. Jiang, C. Chang, and L. Lin, "Piezoelectric actuation of direct-write electrospun fibers," *Sensors and Actuators A: Physical*, vol. 164, no. 1-2, pp. 131–136, 2010.

[13] C. Ribeiro, V. Sencadas, J. L. G. Ribelles, and S. Lanceros-Méndez, "Influence of processing conditions on polymorphism and nanofiber morphology of electroactive poly(vinylidene

fluoride) electrospun membranes," *Soft Materials*, vol. 8, no. 3, pp. 274–287, 2010.

[14] B. Sundaray, F. Bossard, P. Latil, L. Orgéas, J. Y. Sanchez, and J. C. Lepretre, "Unusual process-induced curl and shrinkage of electrospun PVDF membranes," *Polymer*, vol. 54, no. 17, pp. 4588–4593, 2013.

[15] J. Y. Lim, J. Kim, S. Kim, S. Kwak, Y. Lee, and Y. Seo, "Nonisothermal crystallization behaviors of nanocomposites of poly (vinylidene fluoride) and multiwalled carbon nanotubes," *Polymer*, vol. 62, pp. 11–18, 2015.

[16] C. M. Wu and M. H. Chou, "Polymorphism, piezoelectricity and sound absorption of electrospun PVDF membranes with and without carbon nanotubes," *Composites Science and Technology*, vol. 127, pp. 127–133, 2016.

[17] C.-M. Wu, M.-H. Chou, and W.-Y. Zeng, "Piezoelectric response of aligned electrospun polyvinylidene fluoride/carbon nanotube nanofibrous membranes," *Nanomaterials*, vol. 8, no. 6, p. 420, 2018.

[18] M. El Achaby, F. Z. Arrakhiz, S. Vaudreuil, E. M. Essassi, and A. Qaiss, "Piezoelectric β-polymorph formation and properties enhancement in graphene oxide - PVDF nanocomposite films," *Applied Surface Science*, vol. 258, no. 19, pp. 7668–7677, 2012.

[19] S. Yang, X. Cui, R. Guo, Z. Zhang, S. Sang, and H. Zhang, "Piezoelectric sensor based on graphene-doped PVDF nanofibers for sign language translation," *Beilstein Journal of Nanotechnology*, vol. 11, no. 1, pp. 1655–1662, 2020.

[20] K. Nakagawa and Y. Ishida, "Annealing effects in poly(vinylidene fluoride) as revealed by specific volume measurements, differential scanning calorimetry, and electron microscopy," *Journal of Polymer Science: Polymer Physics Edition*, vol. 11, no. 11, pp. 2153–2171, 1973.

[21] L. Fang, C. Xu, W. Zhang, and L. Z. Huang, "The important role of polyvinylpyrrolidone and Cu on enhancing dechlorination of 2,4-dichlorophenol by Cu/Fe nanoparticles: performance and mechanism study," *Applied Surface Science*, vol. 435, pp. 55–64, 2018.

[22] S. Song and S. Lu, "Hydrophobic flocculation of fine hematite, siderite, and rhodochrosite particles in aqueous solution," *Journal of Colloid and Interface Science*, vol. 166, no. 1, pp. 35–42, 1994.

[23] S. H. Wang, Y. Wan, B. Sun, L. Z. Liu, and W. Xu, "Mechanical and electrical properties of electrospun PVDF/MWCNT ultrafine fibers using rotating collector," *Nanoscale Research Letters*, vol. 9, no. 1, pp. 1–7, 2014.

[24] W. A. Yee, A. C. Nguyen, P. S. Lee et al., "Stress-induced structural changes in electrospun polyvinylidene difluoride nanofibers collected using a modified rotating disk," *Polymer*, vol. 49, no. 19, pp. 4196–4203, 2008.

[25] K. H. Lee, H. Y. Kim, H. J. Bang, Y. H. Jung, and S. G. Lee, "The change of bead morphology formed on electrospun polystyrene fibers," *Polymer*, vol. 44, no. 14, pp. 4029–4034, 2003.

[26] H. Fong, I. Chun, and D. H. Reneker, "Beaded nanofibers formed during electrospinning," *Polymer*, vol. 40, no. 16, pp. 4585–4592, 1999.

[27] T. Baby, E. T. Jose, P. C. Thomas, and J. T. Mathew, "A cost effective and facile approach to prepare beadless polycarbonate nanofibers with ultrafine fiber morphology," *Polymer Engineering & Science*, vol. 59, no. 9, pp. 1799–1809, 2019.

[28] S. Singh, V. Singh, and V. B. Prasad, "Single phase bead free PLZT(7/60/40) fibers processed by electrospinning method," *Ceramics International*, vol. 41, no. 2, pp. 2418–2433, 2015.

[29] A. Baji, Y. W. Mai, M. Abtahi, S. C. Wong, Y. Liu, and Q. Li, "Microstructure development in electrospun carbon nanotube reinforced polyvinylidene fluoride fibers and its influence on tensile strength and dielectric permittivity," *Composites Science and Technology*, vol. 88, pp. 1–8, 2013.

[30] V. Sencadas, M. V. Moreira, S. Lanceros-Méndez, A. S. Pouzada, and R. Gregório Filho, "α-to β Transformation on PVDF films obtained by uniaxial stretch," in *Materials science forum*, vol. 514-516, pp. 872–876, Trans Tech Publications Ltd, 2006.

[31] P. Rajesh, S. Bodkhe, S. Kamle, and V. Verma, "Enhancing beta-phase in PVDF through physicochemical modification of cellulose," *Electronic Materials Letters*, vol. 10, no. 1, pp. 315–319, 2014.

[32] A. A. Issa, M. A. A. S. al-Maadeed, M. Mrlík, and A. S. Luyt, "Electrospun PVDF graphene oxide composite fibre mats with tunable physical properties," *Journal of Polymer Research*, vol. 23, no. 11, pp. 1–13, 2016.

[33] R. Gregorio Jr. and N. C. de Souza Nociti, "Effect of PMMA addition on the solution crystallization of the alpha and beta phases of poly(vinylidene fluoride) (PVDF)," *Journal of Physics D: Applied Physics*, vol. 28, no. 2, pp. 432–436, 1995.

[34] A. Hartono, S. Satira, M. Djamal, R. Ramli, H. Bahar, and E. Sanjaya, "Effect of mechanical treatment temperature on electrical properties and crystallite size of PVDF film," *Advances in Materials Physics and Chemistry*, vol. 3, no. 1, pp. 71–76, 2013.

[35] L. Li, M. Zhang, M. Rong, and W. Ruan, "Studies on the transformation process of PVDF from α to β phase by stretching," *RSC Advances*, vol. 4, no. 8, pp. 3938–3943, 2014.

[36] L. Ourry, S. Marchesini, M. Bibani, S. Mercone, S. Ammar, and F. Mammeri, "Influence of nanoparticle size and concentration on the electroactive phase content of PVDF in PVDF–CoFe2O4-based hybrid films," *Physica Status Solidi (A)*, vol. 212, no. 2, pp. 252–258, 2015.

[37] B. Ameduri, "From vinylidene fluoride (VDF) to the applications of VDF-containing polymers and copolymers: recent developments and future trends," *Chemical Reviews*, vol. 109, no. 12, pp. 6632–6686, 2009.

[38] J. H. Lehman, B. Lee, and E. N. Grossman, "Far infrared thermal detectors for laser radiometry using a carbon nanotube array," *Applied Optics*, vol. 50, no. 21, pp. 4099–4104, 2011.

[39] M. S. Hudson, H. Raghubanshi, S. Awasthi et al., "Hydrogen uptake of reduced graphene oxide and graphene sheets decorated with Fe nanoclusters," *International Journal Of Hydrogen Energy*, vol. 39, no. 16, pp. 8311–8320, 2014.

[40] B. Jaffe, W. Cook, and H. Jaffe, "Manufacture of piezoelectric ceramics," *JCPDS*, vol. 41, no. 11, pp. 494–498, 1958.

[41] S. Gao, H. Ao, and H. Jiang, "Properties and performance of general piezoelectric materials on a novel cantilevered energy harvester," in *7th Annual International Conference on Materials Science and Engineering*, Hubei, China., 19-20 April 2019.

[42] C. Chang, Y.-K. Fuh, and L. Lin, "A direct-write piezoelectric PVDF nanogenerator," in *Proceedings of the TRANSDUCERS 2009-2009 International Solid-State Sensors, Actuators and Microsystems Conference*, Denver, CO, USA, 2009.

[43] L. Du, X. Quan, X. Fan, G. Wei, and S. Chen, "Conductive CNT/nanofiber composite hollow fiber membranes with electrospun support layer for water purification," *Journal of Membrane Science*, vol. 596, article ???, 2020.